Physics Letters B 798 (2019) 134960

Contents lists available at ScienceDirect

Physics Letters B

www.elsevier.com/locate/physletb

Evidence of the octupole correlation between the shears bands in ^{142}Eu

Sajad Ali [a], S. Rajbanshi [b,*], R. Raut [c], H. Pai [a], Y.Y. Wang [d], G. Gangopadhyay [e], J. Meng [f], R. Palit [g], Somnath Nag [h], Abhijit Bisoi [i], S. Saha [g,1], J. Sethi [g,2], S. Bhattacharyya [j], S. Chattopadhyay [k], G. Mukherjee [j], A.K. Singh [l], T. Trivedi [m], A. Goswami [a]

[a] Nuclear Physics Division, Saha Institute of Nuclear Physics, HBNI, Kolkata 700064, India
[b] Department of Physics, Presidency University, Kolkata 700073, India
[c] Nuclear Physics Group, UGC-DAE-Consortium for Scientific Research, Kolkata 700098, India
[d] School of Physics and Nuclear Energy Engineering, Beihang University, Beijing, 100191, China
[e] Department of Physics, University of Calcutta, Kolkata 700009, India
[f] State Key Laboratory of Nuclear Physics and Technology, School of Physics, Peking University, Beijing, 100871, China
[g] Department of Nuclear and Atomic Physics, Tata Institute of Fundamental Research, Mumbai 400005, India
[h] Department of Physics, Indian Institute of Technology (BHU), Banaras 221005, India
[i] Department of Physics, Indian Institute of Engineering Science and Technology, Howrah 711103, India
[j] Physics Group, Variable Energy Cyclotron Center, Kolkata 700064, India
[k] High Energy Nuclear & Particle Physics Division, Saha Institute of Nuclear Physics, HBNI, Kolkata 700064, India
[l] Physics Department, Indian Institute of Technology, Kharagpur 721302, India
[m] Department of Pure and Applied Physics, Guru Ghasidas Vishayavidyalaya, Bilaspur 495009, India

ARTICLE INFO

Article history:
Received 21 March 2019
Received in revised form 6 September 2019
Accepted 18 September 2019
Available online 23 September 2019
Editor: D.F. Geesaman

Keywords:
Lifetime measurement
Tilted axis rotation
Principal axis rotation
Octupole correlation
^{142}Eu

ABSTRACT

Two opposite parity dipole sequences (DB I and DB II) in ^{142}Eu have been investigated using the Indian National Gamma Array (INGA), and heavy-ion induced fusion-evaporation reaction, ^{116}Cd(^{31}P, 5n) at E_{Lab} = 148 MeV. The Configurations of these bands are assigned on the basis of tilted axis cranking covariant density functional theory (TAC-CDFT) calculations. The measured $B(M1)$ and $B(E2)$ rates of the DB I and DB II, have been well reproduced within the shears mechanism with the principal axis cranking model (SPAC) calculations leading to the conclusion that these bands have been based on the shears mechanism. The large $B(E1)$ transition rates between DB I and DB II indicate the existence of octupole correlation in ^{142}Eu that has also been corroborated through microscopic multidimensionally-constrained covariant density functional theory (MDC-CDFT) calculations. Thus, the present investigation leads to the novel observation of the presence of octupole correlation between two shears band.

The radiative transitions between non-degenerate energy states in the many-body quantum (fermions) system explicitly reveal the existence of perturbation in the interaction potential. The multipole character of this perturbative potential plays a crucial role in exhibiting a diverse exotic mode of excitation in the different physical systems [1]. The atomic nuclei are the perfect example of the finite many-body quantum systems in which the multipole character of the perturbative Hamiltonian has one to one correspondence to the symmetry-breaking phenomena. The classical viewpoint of the breaking of the symmetry in mass, charge and current distributions leads to the observation of the different types of exotic excitation mechanisms in the level structure of the atomic nuclei. Such multipole modes of excitation depend on the occupancy of the valence particles in the particular orbitals, which leads to various nuclear shapes. For closed-shell nuclei, the shape is perfectly spherical that evolve into axially deformed one for the mid-shell nuclei with a large number of nucleons outside the closed core. The quadrupole term of the perturbative interaction potential is actually responsible for the deformed shape which breaks the rotational symmetry of the nuclear mass (charge) distribution. Such symmetry-breaking leads to the observation of the band structures

* Corresponding author.
E-mail address: subhphy@gmail.com (S. Rajbanshi).
[1] Presently at GSI Helmholtzzentrum für Schwerionenforschung, Darmstadt, Hesse, Germany.
[2] Presently at Department of Chemistry and Biochemistry, University of Maryland, United States.

https://doi.org/10.1016/j.physletb.2019.134960

connected by intraband $E2$ transitions with large $B(E2)$ strengths. The angular momentum in such systems is generated through collective rotation around a principal axis and termed as Principal Axis Rotation (PAR) [2,3]. This mode of excitation has been successfully described in the framework of cranking shell model (CSM) calculations [4]. In this case, the signature is a good quantum number which leads to characteristic staggering in the $\Delta I = 1$ transition energies and in the magnetic dipole transition rates ($B(M1)$). The electric quadrupole transition rates remain nearly constant. On the other hand, for weakly deformed nuclear systems which do not have any preferred axis of rotation, the rotation around a non-principal axis (tilted axis rotation or TAR) is also permissible [5]. In case of such rotation (around a non-principal axis), the signature is no longer a good quantum number [2,5] and the phenomenon manifests itself in sequences of $M1$ transitions with increasing gamma-ray transition energies and decreasing $B(M1)$ and $B(E2)$ values along with the band. Such band structures have been observed for a large number of weakly deformed nuclei across different mass regions and their characteristics have been well explained in the light of the Tilted Axis Cranking (TAC) calculations [6–14].

In a moderately deformed nucleus, however, a high spin band may originate due to an interplay of PAR and TAR. Such a band may simultaneously exhibit the staggering in the $\Delta I = 1$ transition energies and a decrease in the $B(M1)$ rates [15,16]. This is plausible since the $M1$ energy staggering originates due to the influence of the rotationally aligned nucleon while the falling trend of the $B(M1)$ rate is governed by the deformation aligned nucleon.

The occupancy of the valence nucleons in the different shape driving orbitals may lead to the deviation of mass/charge distribution from the spherical symmetry. Most of the deformed nuclei can be adequately described as an axial- and reflection-symmetric spheroid and most of the experimentally observed properties of the resulting band structures can be well reproduced in the calculations. Because such a shape is symmetric under space inversion, all members of the rotational band will have the same parity. However, reflection-asymmetric shapes can also play a role in the excitation mechanism, though they are not as stable as the familiar quadrupole deformations [17]. Such a mode of excitation arises from the interaction between the opposite parity orbitals with $\Delta l = \Delta j = 3$ near the Fermi surface. The breaking of intrinsic reflection symmetry can be due to either static octupole deformation or dynamic octupole correlation. Both these modes of excitation will result in a separation between the center of mass and center of charge of the nucleus, thereby leading to the observation of the alternating parity bands, which are connected by the enhanced $E1$ transitions [18].

In mass $A \sim 140$ region, the $d_{5/2}$ and $h_{11/2}$ proton orbitals lie close together and near the Fermi surface, thereby, can form the basis for octupole interaction. Such pairs of orbitals couple via the Y_{30} operator inducing instability in the mean-field towards β_3 deformations [19]. However, the $d_{5/2}$ and $g_{7/2}$ proton orbitals are almost degenerate in this mass region. This means that octupole correlation effects may be seen over a considerable range of proton numbers and/or might result in a dilution of the octupole effect from the proton orbitals [20].

The ^{142}Eu ($N = 79$, $Z = 63$) nucleus has one proton hole and three neutron holes in $\pi g_{7/2}/d_{5/2}$ and $\nu h_{11/2}$ orbitals, respectively, with respect to the semi-magic nucleus ^{146}Gd ($N = 82$, $Z = 64$). The protons can be easily excited to the $\pi h_{11/2}$ orbital, thus producing a favorable configuration for shears mechanism [12–14, 21–26]. In conjunction, the occupancy of valence nucleons (proton particles and neutron holes) in the shape driving $h_{11/2}$ orbital may lead to the deviation of mass/charge distribution from the spherical symmetry and the possibility of having spheroidal shape leading to rotational sequences [15,27]. In addition, the presence of

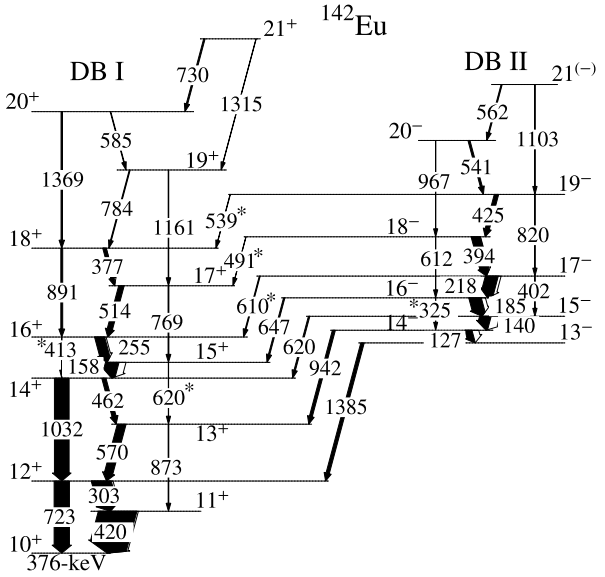

Fig. 1. The partial level scheme of ^{142}Eu obtained in the present work. The γ-ray energies are rounded off to the nearest keV. The newly observed γ-ray transitions are marked by an asterisk.

the proton particles in the $d_{5/2}$ and $h_{11/2}$ orbitals may lead to the appearance of octupole interaction. Therefore, the ^{142}Eu nucleus is a prospective system for exhibiting the collective excitation, shears mechanism and the possible interplay between them, which is indicative from the earlier reported level scheme [28]. Recently, the chirality [29] and octupole correlations in ^{124}Cs [30] have been observed, which offers an example of the interplay between axially asymmetric and reflection-asymmetric shapes. Furthermore, the octupole correlations between multiple chiral doublet bands (MχD) [31] has been reported in ^{78}Br [32], which is supported by the microscopic multidimensionally-constrained covariant density functional theory (MDC-CDFT) [33–35].

In order to explore the existence of the PAR and TAR modes and possible octupole correlation between them, the level structure of ^{142}Eu nucleus has been investigated through the reaction ^{116}Cd(^{31}P, $5n$) at beam energy of E_{Lab} = 148 MeV. The ^{31}P beam was obtained from the Pelletron Linac facility at TIFR, Mumbai. The target was 2.4 mg/cm^2 of ^{116}Cd (99% enriched) on 14.5 mg/cm^2 Pb backing. The de-exciting γ rays were detected using the Indian National Gamma Array (INGA) which consisted of nineteen Compton-suppressed clover detectors (four detectors at 90° and each three at 40°, 65°, 115°, 140°, and 157° with respect to the beam direction) at the time of experiment. The data were sorted [36,37] into several symmetric and asymmetric E_γ - E_γ matrices and E_γ - E_γ - E_γ cube which were then analyzed subsequently with the RADWARE and the INGASORT packages [38–40]. The details of the experiment and data analysis procedures have been described in Refs. [21,22,24].

All the previously observed transitions in the negative parity structure and the positive parity states in ^{142}Eu have been confirmed in the present work from the intensity, DCO ratio (R_{DCO}), ADO ratio (R_θ), mixing ratio and polarization measurements [21, 22,24]. We have rearranged the positive parity states with spins from 10^+ to 20^+ in ^{142}Eu into band DB I whereas the negative parity structure reported earlier [28] has been labeled as DB II (Fig. 1). From the coincidence measurement two newly observed γ transitions of energy 620.3 ($15^+ \rightarrow 13^+$) and 413.0 ($16^+ \rightarrow 14^+$)-keV were placed in DB I. Measured R_θ for 413.0-keV transition was found to be of 1.89(0.21) ($\sim$ 1.6 for pure quadrupole) in agreement with its $E2$ character. Weak nature of 620.3-keV transition

Table 1
Measured transition energies, branching ratio (Br), level lifetime (τ), $B(M1)$ (considering conversion coefficients and mixing ratio of the transitions of interest), $B(E1)$ and $B(E2)$ values of the DB I and DB II and the electric quadrupole and dipole moments (Q_0 and D_0) of the DB II in ^{142}Eu. The upward and downward arrows represent the lower and upper limit of the measured value, respectively.

J_i^π [$\hbar$]	E_γ[a] [keV]	Br [%]	τ [ps]	$B(\sigma\lambda)$[b] [W.u.]	J_i^π [$\hbar$]	E_γ[a] [keV]	Br [%]	τ [ps]	$B(\sigma\lambda)$[b] [W.u.]	Moment
DB I					DB II					
11^+	419.6 (M1)	100(4)	$0.79^{+0.08}_{-0.08}$	$0.55^{+0.06}_{-0.06}$	14^-	126.7 (M1)	49(6)	4.2 $\downarrow$	0.88 $\uparrow$	
						941.6 (E1)	21(3)		0.21×10^{-4} $\uparrow$	2.13[c] $\uparrow$
12^+	303.2 (M1)	56(3)	$0.75^{+0.10}_{-0.13}$	$0.80^{+0.11}_{-0.14}$	15^-	140.4 (M1)	89(8)	3.1 $\downarrow$	1.84 $\uparrow$	
	722.8 (E2)	44(3)		$55.14^{+7.35}_{-9.56}$		620.3 (E1)	11(2)		0.53×10^{-4} $\uparrow$	3.28[c] $\uparrow$
13^+	569.8 (M1)	90(11)	$0.40^{+0.17}_{-0.16}$	$0.38^{+0.16}_{-0.15}$	16^-	184.5 (M1)	89(8)	$1.36^{+0.22}_{-0.24}$	$2.43^{+0.39}_{-0.43}$	
	873.0 (E2)	10(2)		$9.14^{+3.88}_{-3.66}$		325.0 (E2)	1(1)		$37.60^{+6.08}_{-6.64}$	$3.41^{+0.55}_{-0.60}$[d]
						646.6 (E1)	10(2)		$0.98^{+0.16}_{-0.17} \times 10^{-4}$	$4.30^{+0.70}_{-0.76}$[c]
14^+	461.7 (M1)	16(2)	0.90 $\downarrow$	0.06 $\uparrow$	17^-	218.4 (M1)	91(9)	$1.18^{+0.17}_{-0.18}$	$1.95^{+0.28}_{-0.30}$	
	1031.5 (E2)	61(6)		10.76 $\uparrow$		401.8 (E2)	2(1)		$30.01^{+4.32}_{-4.58}$	$2.92^{+0.42}_{-0.45}$[d]
						610.2 (E1)	7(2)		$0.94^{+0.14}_{-0.14} \times 10^{-4}$	$4.14^{+0.60}_{-0.63}$[c]
15^+	157.8 (M1)	98(10)	$3.43^{+0.56}_{-0.49}$	$1.50^{+0.24}_{-0.21}$	18^-	394.3 (M1)	90(9)	$0.89^{+0.15}_{-0.13}$	$0.53^{+0.09}_{-0.08}$	
	620.3 (E2)	2(1)		$1.18^{+0.19}_{-0.17}$		611.5 (E2)	5(1)		$12.18^{+2.05}_{-1.78}$	$1.82^{+0.31}_{-0.27}$[d]
						491.0 (E1)	5(1)		$1.70^{+0.29}_{-0.25} \times 10^{-4}$	$5.51^{+0.93}_{-0.80}$[c]
16^+	254.6 (M1)	98(10)	$1.46^{+0.22}_{-0.19}$	$1.11^{+0.17}_{-0.15}$	19^-	425.4 (M1)	86(10)	$1.17^{+0.25}_{-0.17}$	$0.30^{+0.06}_{-0.04}$	
	413.0 (E2)	1(1)		$10.57^{+1.59}_{-1.38}$		820.2 (E2)	6(1)		$2.56^{+0.55}_{-0.37}$	$0.81^{+0.17}_{-0.12}$[d]
						539.1 (E1)	8(2)		$1.57^{+0.34}_{-0.23} \times 10^{-4}$	$5.22^{+1.11}_{-0.76}$[c]
17^+	513.7 (M1)	89(7)	$0.46^{+0.06}_{-0.05}$	$0.45^{+0.06}_{-0.05}$	20^-	540.7 (M1)	92(24)	$1.10^{+0.17}_{-0.15}$	$0.17^{+0.03}_{-0.02}$	
	768.5 (E2)	11(3)		$16.54^{+2.16}_{-1.80}$		967.0 (E2)	8(3)		$1.59^{+0.25}_{-0.22}$	$0.62^{+0.10}_{-0.09}$[d]
18^+	377.2 (M1)	64(7)	$1.24^{+0.32}_{-0.28}$	$0.30^{+0.08}_{-0.07}$	$21^{(-)}$	562.0 (M1)	80(11)	0.46 $\downarrow$	0.31 $\uparrow$	
	891.1 (E2)	36(5)		$9.58^{+2.47}_{-2.16}$		1103.0 (E2)	20(4)		4.94 $\uparrow$	1.07[d] $\uparrow$
19^+	783.4 (M1)	62(10)	0.74 $\downarrow$	0.06 $\uparrow$						
	1161.2 (E2)	38(7)		4.51 $\uparrow$						
20^+	585.0 (M1)	21(6)	0.81 $\downarrow$	0.04 $\uparrow$						
	1368.6 (E2)	79(12)		3.77 $\uparrow$						

[a] Uncertainty in γ-ray energy is $\pm$ (0.1-0.3)-keV.
[b] Uncertainty in transition strength includes the uncertainty in lifetime only.
[c] Electric dipole moment (D_0) in $10^{-2}efm$.
[d] Electric quadrupole moment (Q_0) in eb.

leads to the tentative multipolarity assignment for the same. The present coincidence measurement also confirms three new weak cross-over 325.0 ($16^- \rightarrow 14^-$), 401.8 ($17^- \rightarrow 15^-$) and 611.5-keV ($18^- \rightarrow 16^-$) $E2$ transitions which have been placed in between the states of DB II. The R_θ values for 325.0- and 401.8-keV transitions were found to be 1.30(21) and 1.43(22), respectively, commensurate with the $E2$ nature of these (cross-over) transitions. Piiparinen et al. had assigned $E1$ multipolarity to the four transitions of energy 1384.8, 941.6, 620.3, 646.6-keV through which dipole band DB II decays into DB I, based on their measured pure dipole character, resulting in a negative parity for DB II [28]. Measured R_{DCO} and R_θ values for the 1384.8, 941.6, 620.3, 646.6-keV transitions are 0.47(7) and 0.66(7), 0.60(13) and 0.51(8), 0.48(8) and 0.68(6), and 0.53(8) and 0.66(7), respectively, thereby indicating their dipole nature ($R_{DCO} \sim 0.5$ and $R_\theta \sim 0.6$ for the pure dipole transition). In the present study, three new γ transitions of energy 610.2 ($17^- \rightarrow 16^+$), 491.0 ($18^- \rightarrow 17^+$) and 539.1 ($19^- \rightarrow 18^+$)-keV, connecting the states of DB I and DB II, have been observed (Fig. 1). The measured R_θ values of the 610.2, 491.0 and 539.1-keV transitions are 0.73(5), 0.68(7) and 0.59(6), respectively in compliance with their dipole character. Out of these seven connecting transitions polarization can be extracted for four transitions (1384.8, 941.6, 620.3- and 646.6-keV). Measured polarization values of the 1384.8, 941.6, 620.3- and 646.6-keV transitions are +0.47(21), +0.34(23), +0.22(14) and 0.46(31), respectively, thereby confirming of their electric dipole nature (polarization is positive for the electric transition). The polarization of the remaining three transitions (610.2 keV, 491.0 keV, and 539.1 keV) could not be evaluated due to the lack of statistics. Nevertheless, the E1 character of these transitions was confirmed through the definitive spin-parity assignments of the respective initial and final states in DB I and DB II.

The level lifetimes of the ten levels (20^+ to 11^+) of DB I and eight levels ($21^{(-)}$ to 14^-) of DB II in ^{142}Eu have been extracted in the present work using the Doppler Shift Attenuation Method (DSAM). The Doppler shape of the transitions at 65°, 90° and 140° have been analyzed simultaneously with the help of the LINESHAPE [41–43] package as per the procedure detailed in Ref. [22]. The 1368.6-keV ($20^+ \rightarrow 18^+$) and 562.0-keV ($21^{(-)} \rightarrow 20^-$) transitions are the highest transitions of the dipole bands DB I and DB II, respectively, for which a clear Doppler shape has been observed in the experimental spectrum, wherefrom the effective lifetimes of 0.81 ps and 0.46 ps have been extracted for the 20^+ and $21^{(-)}$ states, respectively. The 19^+ state of DB I feeds from 20^+ state, topmost level of the DB I and 21^+ state, the band-head of the dipole rotational like band [28]. Therefore the change in structure occurs beyond 20^+ of DB I. For the shake of unknown nature of the side-feeding of the 21^+ state (band-head of dipole rotational like band) an upper limit of the life time of 19^+ state has been extracted. These are then used as the input parameters for obtain-

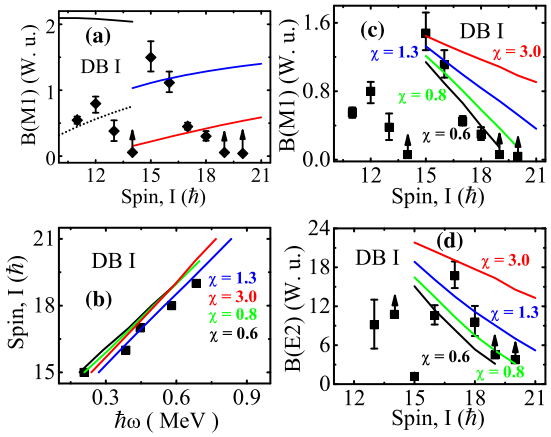

Fig. 2. Comparison of the experimental $B(M1)$ values as a function of spin for the DB I in ^{142}Eu with the theoretical Dönau model (panels (a)) [44]. In panels (a) the solid black lines represent the calculated $B(M1)$ values for before the back bending of DB I. The solid red and blue represents calculated values of $B(M1)$ after the back bending of DB I assuming the proton hole pair occupancy in the nearly degenerate $d_{5/2}$ and $g_{7/2}$ orbitals, respectively. A better fit to the B(M1) values of the band DB I before back bending can be obtained where the two quasiparticles are treated as a common structure assuming the "common" two quasipaticle g factor (g^{2QP}), alignment (i^{2QP}) and projection along the symmetry axis (K^{2QP}) as +1.35, 4$\hbar$ and 5$\hbar$, respectively [45] represented by dotted line in panel (a). Panels (b), (c) and (d) show the comparison of the ω, $B(M1)$ and $B(E2)$ values against spin (I) for the DB I in ^{142}Eu with the modified SPAC model calculations [46] represented by the solid red (χ = 3.0), blue (χ = 1.3), green (χ = 0.8) and black (χ = 0.6) lines.

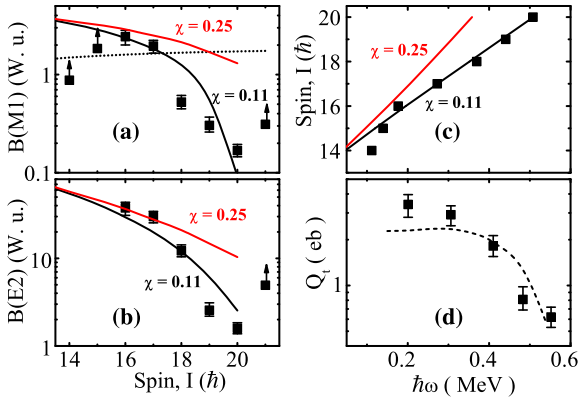

Fig. 3. Panels (a), (b) show the comparison of the experimental $B(M1)$ and $B(E2)$ values for the DB II in ^{142}Eu with the SPAC (solid line) calculations. In panel (a) the dotted line represents the theoretical Dönau model [44] calculation. In the panel (c) the variation of spin (I) against the rotational frequency (ω) is compared with the SPAC calculations. Experimental Q_t values of DB II are compared with the TRS calculations [47,48] (dashed line) in panel (d). The parameters used in the SPAC calculations are j_1 = 10$\hbar$, j_2 = 8$\hbar$, g_1 = 1.21, g_2 = -0.014, Q_{eff} = 7.10 eb and Q_{col} = 0.50 eb [21]. The solid black and red lines represent the SPAC calculation with χ = 0.11 and 0.25, respectively.

ing the level lifetimes of the lower-lying states of the cascades. It is to be pointed out that in some cases the level of interest has been populated by more than one gamma transitions and the respective states have a finite lifetime. For example, 19^- state of DB II, which decays via 425.4-keV transition, is populated by the 540.7- and 1103.0-keV transitions de-exciting the 20^- and $21^{(-)}$ levels of DB II, respectively. This information has been incorporated in the analysis by replacing the lifetime of the (top) feeding in-band level by the intensity weighted average of the lifetimes of the two feeding states. For the 14^+ level of the DB I, several transitions have been found to depopulate from the state. It is difficult to define proper branching ratio and side-feeding intensity parameters to the lineshape fitting of the transition depopulating this state. Therefore, an upper limit of the level lifetime for this state has been extracted. A similar situation arises for the 14^- and 15^- states in DB II and an upper limit of the level lifetime has been estimated for these states as well. The extracted level lifetimes and the corresponding reduced transition probabilities $B(M1)$, $B(E1)$ and $B(E2)$ values for the bands DB I and DB II are recorded in Table 1.

M. Piiparinen et al. had measured the lifetimes of the two levels (14^+ and 16^+) in DB I and five levels (14^- to 18^-) in DB II using the plunger technique [28]. The lifetimes were considerably larger (roughly by a factor of 2) than the present DSAM results, which are well beyond the uncertainties of both measurements. It may be noted that the LINESHAPE analysis gives a limit for the highest level of the band, and uses it later as an input parameter when calculating the lower levels in the band. This implies that the uncertainty for the highest level carrying through each lower level that is being analyzed and added to their actual measured uncertainty in a compound way. This may produce the discrepancy between the lifetimes obtained from the present DSAM measurements and the previous plunger techniques. In addition, the deviation may also arise due to the presence of the systematic uncertainty in the lifetime and owing to the newly observed cross-over E2 transitions the side-feeding intensity of the levels of interest are differs against their respective values as reported by M. Piiparinen et al..

However, in both cases, the measured lifetime and corresponding transition probabilities ($B(M1)$, $B(E1)$ and $B(E2)$ values) and their variation with spin exhibits the same characteristic trend, possibly leading to the same interpretation of the bands and suggested octupole correlations, detailed in the next section.

The measured reduced transition rates ($B(M1)$ and $B(E2)$) decrease with increasing spin for both DB I and DB II. The numerical values for the $B(M1)$ rates calculated through the geometric Dönau model [44] have been compared with the experimental values for DB I and DB II in Fig. 2 (a) and Fig. 3 (a), respectively. The parameters used for these calculations are tabulated in Table 2. These calculations assume PAR and it clearly fails to reproduce the observed falling trend thereby indicating that both the dipole bands may originate due to the shears mechanism. Such behavior has been observed in a number of nuclei in this mass region [9,12–14, 21,22,24,49].

This prompted us to examine the behavior of the angular momentum against the rotational frequency for the DB I and DB II in the framework of the tilted axis cranking covariant density functional theory (TAC-CDFT) formalism [50–55]. The comparison with the data is shown in Fig. 4. For DB I, the calculated results based on $\pi h^1_{11/2} \otimes \nu h^{-1}_{11/2}$ configuration, similar to that assigned by Piiparinen et al. [28], with pairing correlation before backbending and $\pi h^1_{11/2}(g_{7/2}/d_{5/2})^{-2} \otimes \nu h^{-1}_{11/2}$ configuration without pairing after backbending are in good agreement with the data. Similarly, for DB II, the experimental results are well reproduced with $\pi h^2_{11/2}(g_{7/2}/d_{5/2})^{-1} \otimes \nu h^{-1}_{11/2}$ configuration. These calculations show that the tilt angle for DB I and DB II are $\sim 25°$ and $\sim 51°$, respectively at 15$\hbar$. This indicates a substantially larger contribution of the collective rotation in DB I as compared to DB II, since both the bands extend up to $I \sim 20\hbar$, which in turn, might explain the origin of the energy staggering observed in DB I. The smaller $B(M1)$ rates of DB I than DB II (as tabulated in Table 1) also indicates a smaller tilt angle for DB I.

The quantitative measures of the contribution of core rotational angular momentum in the magnetic rotational (MR) bands have been investigated by incorporating a dimensionless parameter, χ (representative of the contribution of the angular momentum produced by the rotation of the deformed core with respect to the shears mechanism), in the shears mechanism with principal axis cranking (SPAC) model calculations [46]. The to-

Table 2
Parameters used in the calculation of $B(M1)$ transition rates using Dönau geometric model [16,44]. DAL and RAL corresponds to the deformed aligned and rotational aligned counterpart of the quasi-particles, respectively.

Band	K	DAL configuration	i_x^1 ($\hbar$)	$g^{(1)}$ [56]	RAL configuration	i_x^2 ($\hbar$)	$g^{(2)}$ [56]
DB I[a]	6	$\pi[h_{(11/2)}]\frac{11}{2}^-$	$\frac{1}{2}$	+1.21	$\nu[h_{(11/2)}]\frac{1}{2}^-$	5.5	−0.21
DB I[b]	7	$\pi[h_{(11/2)}]\frac{11}{2}^-$	0.5	+1.21	$\nu[h_{(11/2)}]\frac{1}{2}^- \otimes \pi[d_{(5/2)}]\frac{3}{2}^+ \otimes \pi[d_{(5/2)}]\frac{1}{2}^+$	9.5	+1.062
DB I[b]	7	$\pi[h_{(11/2)}]\frac{11}{2}^-$	0.5	+1.21	$\nu[h_{(11/2)}]\frac{1}{2}^- \otimes \pi[g_{(7/2)}]\frac{3}{2}^+ \otimes \pi[g_{(7/2)}]\frac{1}{2}^+$	11.5	+0.534
DB II	7	$\pi[h_{(11/2)}]\frac{11}{2}^- \otimes \pi[h_{(11/2)}]\frac{9}{2}^-$	2.0	+1.21	$\nu[h_{(11/2)}]\frac{1}{2}^- \otimes \pi[g_{(7/2)}]\frac{1}{2}^+$	9.0	+0.255

[a] Configuration before band crossing.
[b] Configuration after band crossing.

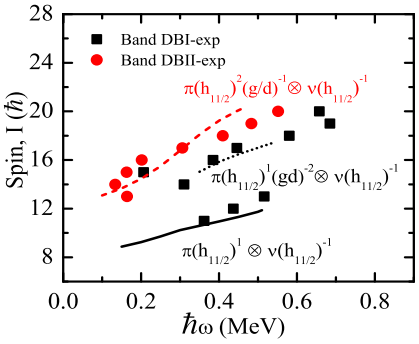

Fig. 4. Total angular momenta calculated by TAC-CDFT including with and without pairing correlations, represented by solid and dashed lines, respectively, for DB I and DB II in ^{142}Eu as a function of rotational frequency, in comparison with the data.

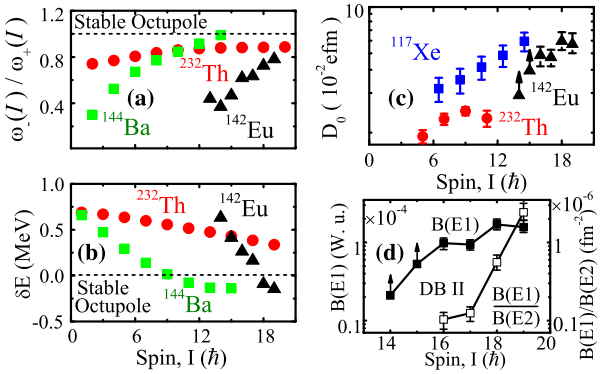

Fig. 5. Variation of δE, $\omega^-(I)/\omega^+(I)$ ratio and D_0 against spin (I) for the bands in ^{142}Eu, ^{117}Xe, ^{232}Th and ^{144}Ba in Figs (a), (b) and (c), respectively. Panel (d) shows the dependence of $B(E1)/B(E2)$ against spin (I).

tal Routhian surface (TRS) calculation [47,48] exhibits the oblate minima for the configurations $\pi h^1_{11/2}(g_{7/2}/d_{5/2})^{-2} \otimes \nu h^{-1}_{11/2}$ and $\pi h^2_{11/2}(g_{7/2}/d_{5/2})^{-1} \otimes \nu h^{-1}_{11/2}$ assigned to the upper part of DB I and DB II in ^{142}Eu, respectively. The modified SPAC model calculations have been performed assuming the oblate deformed shape with an unstretched condition of j_1 = 4.5$\hbar$, j_2 = 11.5$\hbar$ using the values of the g-factors for the particle and hole sectors as g_1 = +1.21 and g_2 = -0.014, respectively, for the upper part of DB I [21]. The collective and quasiparticle quadrupole moment parameters used in this modified SPAC calculation are Q_{col} = 0.50 eb and Q_{eff} = 1.50 eb, respectively. The experimental $B(M1)$ and $B(E2)$ values are reproduced for different values of χ as depicted in Figs. 2 (c) and (d). These figures show that the lower spin ($I \sim 15\hbar$) states are generated for higher value of χ ($\sim$ 3.0) whereas small values of χ ($\sim$ 0.6) are responsible for the higher angular momentum states after the back bending of DB I. This indicates that the angular momentum generated after the band crossing of DB I has large core contribution ($\sim$ 75%) at lower spin ($\sim 15\hbar$) which decreases smoothly along the band ($\sim$ 38% at $I \sim 19\hbar$). The experimental Routhian and the transition rates in DB II have also been well reproduced in the modified SPAC model calculation with a very small collective contribution ($\sim$ 10%) as shown in Fig. 3. This clearly indicates that the DB II has been originated with the "shears mechanism" while the states after the back bending in DB I are generated due to the interplay of the PAR with the MR phenomenon representing the TAR.

The DB II decays to the DB I through the strong $E1$ transitions with large $B(E1)$ ($\sim 10^{-4}$ $W.u.$) and $B(E1)/B(E2)$ transition rates (Table 1, Fig. 5 (d)). Such large transition rates are comparable to the values observed in the opposite parity (octupole) bands of ^{124,125}Ba [57], ^{117}Xe [58] and ^{124}Cs [30]. Thus, the bands DB I and DB II differing by 3$\hbar$ at the band-head spin and connected through $E1$ transitions indicate a reflection asymmetric shape. The shape transition from reflection symmetric at low spin to reflection asymmetric at medium spin induced by rotation is plausible in ^{142}Eu. Such symmetry breaking induced by rotation has been observed in ^{148}Sm and ^{146}Nd [59] and supported by theoretical consideration [60].

To get a better understanding of the DB I and DB II the energy displacement $\delta E(I)$ and the rotational frequency ratio $\omega_-(I)/\omega_+(I)$ [18] have been calculated. These values sharply approach the stable octupole limit with increasing spin and overlap with the observed octupole deformed bands in ^{144}Ba [61] and vis-à-vis to the small variation of the octupole correlated bands in ^{232}Th [62] (Figs. 5 (a), (b)). Magnitude of the extracted intrinsic dipole moment D_0 from the measured $B(E1)$ values exhibit a slow increase from $4.30^{+0.70}_{-0.76} \times 10^{-2} efm$ at I^π = 16$^-$ to $5.51^{+0.93}_{-0.80} \times 10^{-2} efm$ at I^π = 19$^-$ in the DB II, which is similar to the octupole correlated bands in ^{117}Xe and ^{232}Th (5 (c)). This slow variation of D_0 is in contrast with the sharp increase of the $B(E1)/B(E2)$ rate (Fig. 5 (d)) which arises due to the rapid falling of the Q_t values with spin due to TAR (Fig. 3 (d)). This indicates that a dynamical octupole correlation between the $d_{5/2}$ and $h_{11/2}$ proton orbitals near the Fermi surface may exist in ^{142}Eu [18] and is the first experimental evidence of such a correlation between two shears band. To further check the feasibility of the observed octupole correlations in ^{142}Eu, the potential energy surface in the β_{20} - β_{30} plane has been calculated in the framework of a microscopic MDC-CDFT formalism [33–35] with the effective interaction PC-PK1 [55] (Fig. 6). The potential energy surface is very soft with respect to the shape degree of freedom β_{30}, which further upholds the propositions of octupole correlations in ^{142}Eu. Thus, the present investigation leads to the novel observation of two opposite parity bands, originating due to the interplay of PAR and TAR and interacting through the octupole interaction potential.

In summary, the two opposite parity dipole bands DB I and DB II in ^{142}Eu have been investigated. The configurations $\pi h^1_{11/2} \otimes \nu h^{-1}_{11/2}$ and $\pi h^1_{11/2}(d_{5/2}/g_{7/2})^{-2} \otimes \nu h^{-1}_{11/2}$ have been assigned to DB I before and after band crossing, respectively, whereas the

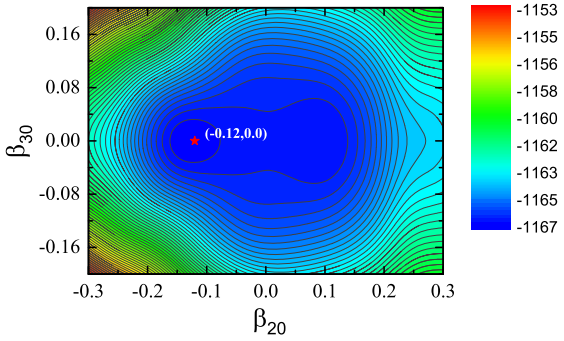

Fig. 6. The potential energy surface of ^{142}Eu calculated by the MDC-CDFT approach [33–35]. The contour separation is 0.25 MeV. The pentagram corresponds to the point of the minimum energy.

configuration for DB II is $\pi h^2_{11/2}(d_{5/2}/g_{7/2})^{-1} \otimes \nu h^{-1}_{11/2}$. The DB I has been established to be resulting from the interplay of PAR with MR phenomena representing the TAR while DB II emerges from the shears mechanism. The measured electric dipole moment (D_0), energy displacement $\delta E(I)$ and rotational frequency ratio $\omega_-(I)/\omega_+(I)$ associated with the DB I and DB II as well as potential energy surface calculation in the framework of MDC-CDFT, indicate an octupole correlation in ^{142}Eu presumably due to availability of valence nucleons (protons) in the $d_{5/2}$ - $h_{11/2}$ orbitals near the Fermi surface. This is the first experimental evidence of octupole correlation between two shears band.

Acknowledgements

The authors gratefully acknowledge financial support from the Department of Science & Technology (DST) for the INGA Project (Project No. IR/S2/PF-03/2003-II). We would like to acknowledge help from all INGA collaborators and the participants during the experiment. We are thankful to the TIFR-BARC Pelletron-LINAC staff for smooth operation of the accelerator facility. G.G. acknowledges support provided by the University Grants Commission, Departmental Research Support (UGC-DRS) Program [Program No. F.530/16/DRS-II/2015(SAP-I)]. S. R. would like to acknowledge the financial assistance from the University Grants Commission - Minor Research Project (No. PSW-249/15-16 (ERO)) and the FRPDF grant of Presidency University Kolkata, India. A. K. S. would also like to acknowledge MHRD, Govt. of India for financial support. H. P. is grateful for the support of the Ramanujan Fellowship research grant under SERB-DST (SB/S2/RJN-031/2016). Y. Y. W. and J. M. would like to acknowledge the support of the National Key R&D Program of China (Contract No. 2018YFA0404400 and No. 2017YFE0116700), the National Natural Science Foundation of China (Grants No. 11621131001 and No. 11875075).

References

[1] V.A. Dzuba, V.V. Flambaum, et al., Phys. Rev. A 93 (2016) 052517.
[2] M.J.A. de Voigt, J. Dudek, Z. Szymański, Rev. Mod. Phys. 55 (1983) 949.
[3] Stefan Frauendorf, Rev. Mod. Phys. 73 (2001) 463.
[4] W. Nazarewicz, J. Dudek, R. Bengtsson, T. Bengtsson, I. Ragnarsson, Nucl. Phys. A 435 (1985) 397–447.
[5] S. Frauendorf, Nucl. Phys. A 557 (1993) 259c–276c.
[6] H. Hübel, Prog. Part. Nucl. Phys. 54 (2005) 1–69.
[7] D.G. Jenkins, et al., Phys. Lett. B 428 (1998) 23–30.
[8] D.G. Jenkins, et al., Phys. Rev. Lett. 83 (1999) 500.
[9] R.M. Clark, et al., Phys. Rev. Lett. 82 (1999) 3220.
[10] H. Schnare, et al., Phys. Rev. Lett. 82 (1999) 4408.
[11] Sham S. Malik, Priyanka Agarwal, Ashok K. Jain, Nucl. Phys. A 732 (2004) 13–23.
[12] A.A. Pasternak, et al., Eur. Phys. J. A 37 (2008) 279–286.
[13] E.O. Podsvirova, et al., Eur. Phys. J. A 21 (2004) 1–6.
[14] A.A. Pasternak, et al., Eur. Phys. J. A 23 (2005) 191–196.
[15] R.M. Lieder, et al., Eur. Phys. J. A 13 (2002) 297–305.
[16] P. Datta, et al., Phys. Rev. C 67 (2003) 014325.
[17] P.A. Butler, W. Nazarewicz, Rev. Mod. Phys. 68 (1996) 349.
[18] A.V. Afanasjev, S. Mizutori, Z. Phys. A 353 (1995) 267–271.
[19] J.R. Jongman, et al., Phys. Rev. C 50 (1994) 3159.
[20] Raymond K. Sheline, Prakash C. Sood, Prog. Theor. Phys. 81 (1989) 5.
[21] S. Rajbanshi, et al., Phys. Rev. C 89 (2014) 014315.
[22] S. Rajbanshi, et al., Phys. Rev. C 90 (2014) 024318.
[23] S. Rajbanshi, et al., Phys. Lett. B 748 (2015) 387–391.
[24] S. Rajbanshi, et al., Phys. Rev. C 94 (2016) 044318.
[25] Sajad Ali, et al., Phys. Rev. C 96 (2017) 021304(R).
[26] S. Rajbanshi, et al., Phys. Lett. B 782 (2018) 143–148.
[27] Priyanka Agarwal, et al., Phys. Rev. C 76 (2007) 024321.
[28] M. Piiparinen, et al., Nucl. Phys. A 605 (1996) 191–268.
[29] S. Frauendorf, J. Meng, Nucl. Phys. A 617 (1997) 131.
[30] K. Selvakumar, et al., Phys. Rev. C 92 (2015) 064307.
[31] J. Meng, J. Peng, S.Q. Zhang, S.-G. Zhou, Phys. Rev. C 73 (2006) 037303.
[32] C. Liu, et al., Phys. Rev. Lett. 116 (2016) 112501.
[33] B.N. Lu, E.G. Zhao, S.-G. Zhou, Phys. Rev. C 85 (2012) 011301(R).
[34] J. Zhao, B.N. Lu, E.G. Zhao, S.-G. Zhou, Phys. Rev. C 86 (2012) 057304.
[35] B.N. Lu, J. Zhao, E.G. Zhao, S.-G. Zhou, Phys. Rev. C 89 (2014) 014323.
[36] R. Palit, et al., Nucl. Instrum. Methods A 680 (2012) 90.
[37] H. Tan, et al., in: Nuclear Science Symposium Conference Record 2008, IEEE, Washington, DC, 2008, p. 3196.
[38] D.C. Radford, Nucl. Instrum. Methods Phys. Res., Sect. A 361 (1995) 297.
[39] D.C. Radford, Nucl. Instrum. Methods Phys. Res., Sect. A 361 (1995) 306.
[40] R.K. Bhowmik, INGASORT manual (private communication).
[41] J.C. Wells, N.R. Johnson, LINESHAPE: A Computer Program for Doppler Broadened Lineshape Analysis, Report No. ORNL - 6689, 44, 1991.
[42] L.C. Northcliffe, R.F. Schilling, Nucl. Data Tables A 7 (1970) 233.
[43] N.R. Johnson, et al., Phys. Rev. C 55 (1997) 652.
[44] F. Dönau, Nucl. Phys. A 471 (1987) 469–488.
[45] P. Petkov, et al., Nucl. Phys. A 640 (1998) 293–321.
[46] S. Rajbanshi, et al., Phys. Rev. C 98 (2018) 061304(R).
[47] W. Nazarewicz, J. Dudek, R. Bengtsson, T. Bengtsson, I. Ragnarsson, Nucl. Phys. A 435 (1985) 397.
[48] W. Nazarewicz, M.A. Riley, J.D. Garrett, Nucl. Phys. A 512 (1990) 61.
[49] A.O. Macchiavelli, et al., Phys. Rev. C 57 (1998) R1073.
[50] P.W. Zhao, J. Peng, H.Z. Liang, P. Ring, J. Meng, Phys. Rev. Lett. 107 (2011) 122501.
[51] J. Meng, J. Peng, S.Q. Zhang, P.W. Zhao, Front. Phys. 8 (2013) 55.
[52] P.W. Zhao, N. Itagaki, J. Meng, Phys. Rev. Lett. 115 (2015) 022501.
[53] P.W. Zhao, et al., Phys. Lett. B 699 (2011) 181.
[54] P.W. Zhao, et al., Phys. Rev. C 92 (2015) 034319.
[55] P.W. Zhao, et al., Phys. Rev. C 82 (2010) 054319.
[56] T. Lonnröth, et al., Z. Phys. A 317 (1984) 215.
[57] P. Mason, et al., Phys. Rev. C 72 (2005) 064315.
[58] Z. Liu, et al., Eur. Phys. J. A 1 (1998) 125.
[59] W. Urban, et al., Phys. Lett. B 258 (1991) 293.
[60] W. Nazarewicz, S.L. Tabor, Phys. Rev. C 45 (1992) 2226.
[61] J.H. Hamilton, et al., Acta Phys. Pol. B 32 (2001) 957.
[62] B. Ackermann, et al., Nucl. Phys. A 559 (1993) 61–82.